Investigation of low dimensional GeSe structures for optoelectronics

TONG XUN JIE

A0098707N

A THESIS SUBMITTED FOR THE FULFILLMENT FOR THE DEGREE IN BACHELOR OF SCIENCE (HONOURS)

DEPARTMENT OF PHYSICS

NATIONAL UNIVERSITY OF SINGAPORE

AY2015/16

Acknowledgements

This final year project has indeed been an experience. I've gotten to live the life of a researcher, experienced the constantly nagging voice in my head asking 'why?', faced the setbacks and the frustrations but also the moments when things appeared to all come together and experienced and the joy of understanding something new.

My deepest gratitude to Professor Sow Chorng Haur, my supervisor, for the opportunity to carry out this project under him and the guidance he has provided over the course of the project. He has also been very approachable and though being a busy man, makes time to talk and guide us through our project.

I'd also like to thank Dr. Lu Junpeng, my mentor, for the guide and the support that he has provided. He has been the person to have walked alongside me whilst I was new to the lab, all the lab equipment and to advise me on my project scope when the options seemed too many. It has indeed been a great pleasure and an honor to have seen him work, and gotten to work with him.

Apart from them, there have been people whom have been deeply supportive whilst I was carrying out my project. The people in my lab, Dr. Lim Xiaodai Sharon, Miss Gong Lili, Mr. Lim Kim Yong, Dr. Zheng Minrui, whom have helped and guided me on both the small things and big, and whom have been a friend, Hu Zhenliang, Cyrus Poon, Jin Feng and Dan Jiadong.

I'd like to thank my parents, my physics course mates, especially Tan Tu Guang, Roslyn Ang, Janet Lim, Hew Kai Ming, Samuel Seah, Seng Leng Kiat and Roger You, and the Varsity Christian Fellowship friends for watching out and praying for me amongst others for the support and the help provided during the course of the project.

Most Importantly, I thank God for seeing me through this project.

Contents

Abstract

Germanium Selenide (GeSe) is one of the group-IV monochalcogenides, which form a family within the wider group of semiconductors known as 'phosphorene analogues'. In this project, we synthesize GeSe nanostructures via a vaporization condensation recrystallization method onto polished Si substrate. The synthesized nanostructures were then characterized using SEM and AFM for morphology and also to look for hints that may point to a specific growth mechanism, UV-Vis spectroscopy to study band features and to determine the band gap, and Raman spectroscopy to study the phonon modes of the synthesized structures. We then took 1D GeSe structures and fabricated them into devices using photolithography to test the optoelectronic properties of the GeSe structures.

1. Introduction

In recent years, there has been increased interest in 2D nanostructures as prospective candidates for applications such as photovoltaics, field effect transistors, batteries and photodetectors among other purposes. One of the most studied materials is Graphene, which has excellent performance as sensors and optoelectronic devices. However, graphene doesn't have a bandgap resulting in weak light absorption and fast recombination of the charge carriers generated when light is absorbed. The materials that are being studied in the light of this problem include Transition Metal Dichalcogenides (TDMCs) and phosphorene amongst others. [1, 2]

Phosphorene is a single layer of black phosphorous which, similar to graphene, is made up of layers of phosphorous atoms held strongly by covalent bonds with three other phosphorous atoms to form a puckered honeycomb structure. Van der Waals forces are the main interaction between layers. [3] The puckered honeycomb structure results in phosphorene having an orthorhombic structure different from both graphene and TMDCs, such as superior flexibility when under strain and a giant thermoelectric coefficient.

Group-IV monochalcogenides (SnS, SnSe, GeS, and GeSe), are a family of semiconductor materials known as 'phosphorene analogues'. In α-phase, these materials share a lattice structure similar to phosphorene (see Fig. 1.1) which exhibit graphite-like structure in having strong covalent bonds between atoms that are on the same layer, and are held by Van Der Waals forces between layers. [2] Furthermore, within this group of materials, Ge based chalcogenides (GeS and GeSe) have relatively abundant source materials and are low toxicity which makes them a viable candidate to study. [1] GeSe has been synthesized and

experimented in the lab before and the results look promising. [4] As such, we shall attempt to build upon existing research to understand GeSe nanostructures more.

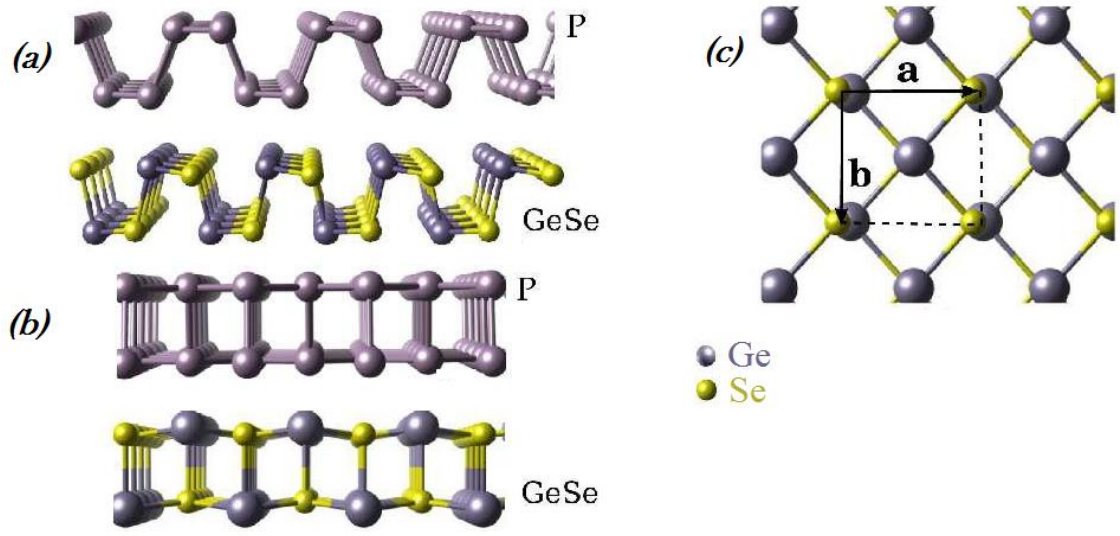

Fig. 1.1 Illustration of lattice structure of Phosphorene and single layer GeSe. (a) The lattice structure of phosphorene and GeSe in the x-z plane. (b) The lattice structure of phosphorene and GeSe in the x-z plane. (c) The lattice structure of GeSe in the x-y plane. Directions a and b correspond to the x and y direction respectively. Image edited from [2]

I. Semiconductors and Conductivity

Semiconductors are a class of materials that have conductivity at room temperature within the range of 10^{-2} to 10^{9} ohm-cm. Their resistivity is highly dependent on temperature and is less than insulators. To explain conductivity of materials, we can look to band gap theory.

1. Band gap

From the Kronig-Penny model, the band structure arises when we consider the nearly free electron model where electrons are treated as perturbed weakly in a periodic function of ion cores. Bragg diffraction is a characteristic feature of waves propagating in crystals. When this is factored in, smooth wave-like solutions of the Schrödinger's equation no longer exist, but result in forbidden energy bands between allowed energy levels. [5]

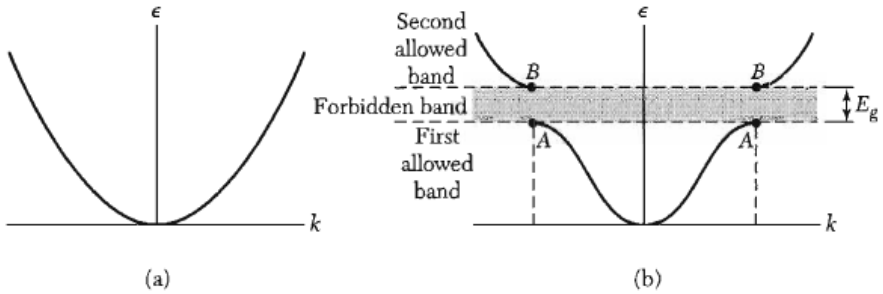

Fig. 1.2 Plot of Energy ε versus wavevector K for (a) free electron and (b) in a mono-atomic linear layer with constant lattice constant. An energy gap is formed between allowed energy levels. Other energy gaps are found at higher energies. Image obtained from [5]

At absolute zero, electrons take the lowest energy configuration, so all the states in the lower band (valence band) are filled and all the higher energy bands (conduction band) are empty. The bandgap energy, E_g, is the width of the forbidden energy band. [6] As temperatures increase, a few valence band electrons may be excited into the conduction band and creating empty states in the valence band. If an electron moves in to fill up the empty state, it creates another empty state elsewhere, and as another electrons moves in to fill up the new empty state, another new empty state is formed. We can thus think of the movement of empty states as equivalent to a positive charge carrier moving, and we call this charge carrier a hole. [6]

Each crystal lattice would have its own energy band structure. For conductivity, we need mobile charge carriers. When an electric field is applied, if there are no charge carriers moving, there will be no current. In a very simplified picture (refer to Fig. 1.3) of how energy bands affect conductivity, we can think of insulators as having their energy bands either completely filled or empty, with no movement of charge carriers, insulators have low conductivity. As for metals, we can think of the allowed energy bands as being only partially filled. This results in availability of many available electrons and holes to carry charges, resulting in high conductivity. As for semiconductors, we can think of an energy band having few electrons near the bottom of the band. As an electric field is applied, electrons gain energy and carry charges. Alternatively, we can think of an energy band as almost being completely filled. When electric field is applied, the empty states become holes. These are both possible scenarios for semiconductors. [6]

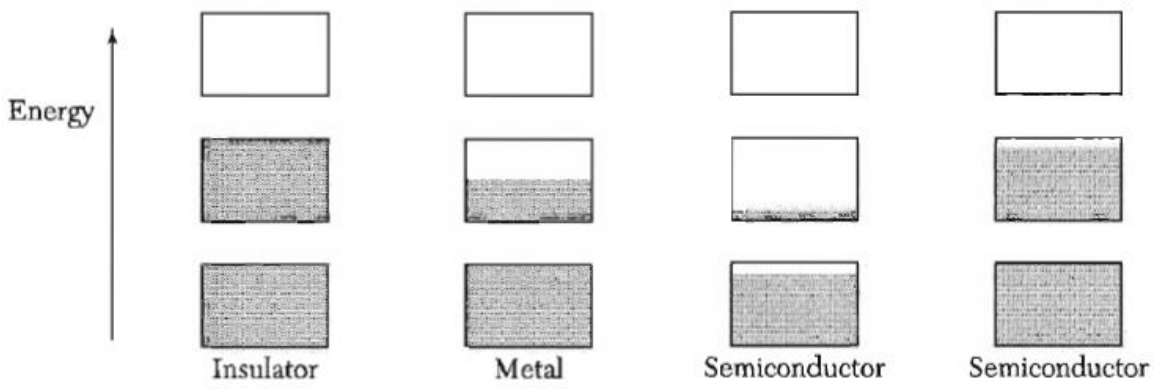

Fig. 1.3 An illustration of band energy configurations in different materials. Electron filled states are shaded. The semi-conductor band energy for n-type semiconductors is illustrated on the left whilst band energy for p-type semiconductors is illustrated on the right. Image referenced from [5]

2. Direct and Indirect Band gaps

The intrinsic carrier concentrations are related to the ratio of the energy difference between the conduction and valence bands, and the temperature. To improve conductivity, electrons need to be excited from valence band to the conduction band, generating an electron and a hole as mobile charge carriers. This could be achieved by either a direct absorption process where a the energy from a photon excites an electron directly to form an electron hole pair due to alignment of the lowest point of the conduction band and the highest point of the valence band in k-space (direct band gap), or an indirect absorption process where due to the misalignment of the lowest point of the conduction band and the highest point of the valence band (indirect band gap) a photon cannot directly excite an electron to the conduction band and requires assistance from phonon vibrations [5]

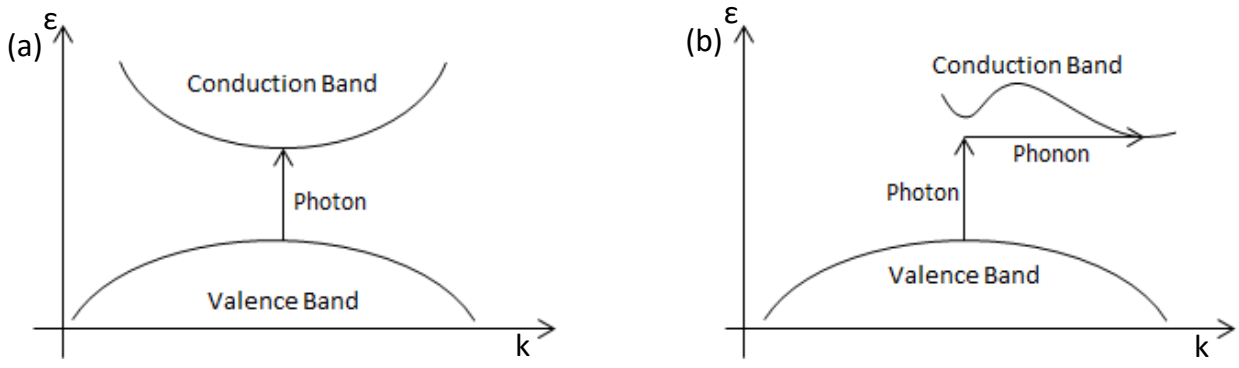

Fig. 1.4 Image showing band structures with direct and indirect band gaps. (a) Shows a direct band gap transition whilst (b) shows an indirect band gap transition

The band features of GeSe have been calculated previously by Lídia C. Gomes and A. Carvalho and the findings have been published in a paper. [2] GeSe is a narrow band IV-VI p-

type semiconductor with an indirect band gap. The band gap has been experimentally determined to be 1.14 [7]

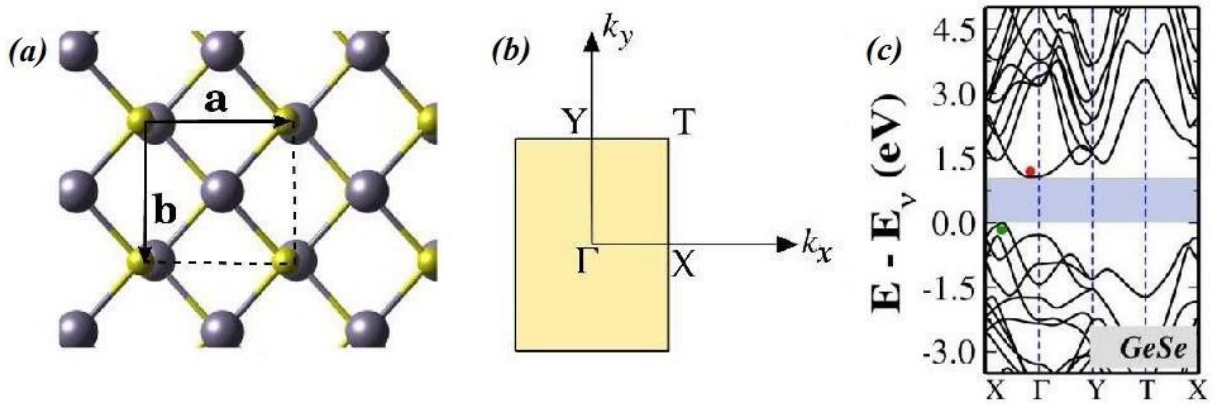

Fig. 1.5 Depiction of Band Gap of GeSe (a) depicts the lattice structure in the x-y plane. (b) The respective BZ and high symmetry points Γ, X, T, and Y and (c) Previously calculated band features of Bulk GeSe from an earlier paper. GeSe has an indirect bandgap. Images taken from [2]

II. Sample Preparation

We tried two methods of preparing samples of GeSe for device testing. The scotch tape exfoliation of high purity GeSe ingots did not yield suitable results. The samples obtained were too small to make devices from.

The other method was using Vaporization–Condensation–Recrystallization (VCR) process. Using Vapour Deposition technique to grow nanostructures allow us to overcome problems faced by more traditional methods, such as exfoliation, which allows limited control over nanostructures obtained, or synthetic solvent methods, which may result in adsorption of solvent at the surface. However, as the chalcogenides are very reactive, we cannot use catalyst to assist or control the growth process, resulting in growth parameters having a strong influence on the outcome of the synthesis process. [8].

VCR is a method of synthesizing materials which is done by generating vapors of the powdered precursors at an elevated temperature and then subsequently a condensation of the vapors on a solid substrate at a lower temperature region. At the lower temperature regions, precursor-specific recrystallization takes place and low dimensional structures can be synthesized. One key advantage of using the VCR technique is that the resulting assembled structures generally possess high crystallinity. [9] VCR is actually modified Vapour to Solid (VS) process and most of the mechanisms that VS processes do apply to VCR. However, VCR processes seem to have more specific vaporization and solidification pathways. The schematic of a VCR process is as shown below. (Fig. 1.6)

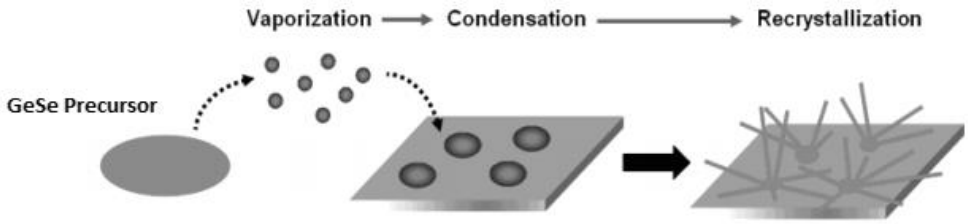

Fig 1.6 VCR process schematic. Image edited from [10]

III. MOSFET device

A transistor is in general a three-terminal device where the resistance between two of the contacts is controlled by the third. In a FET, this resistance is controlled by applying an electric field through a capacitor. Conventionally, the current flows from the source to the drain and the terminal that controls the electric field is called the gate. FETs have a wide array of features for application in digital integrated circuits, analog switching, high-input-impedance amplifiers, and microwave amplifiers.

There are many different classes of FET devices, some FETs are made by using a schottky barrier or a p-n junction to form the capacitance layer (JFET and MESFET), and others would be done so by means of an insulator between the gate and the channel. [11] The device that we will focus on would be a MOSFET (metal-insulator-semiconductor FET) which uses a layer of oxide to act as the insulator layer(See Fig. 1.7) This is achieved practically by applying a potential onto the Si in the substrate below the SiO_2 layer. [11]

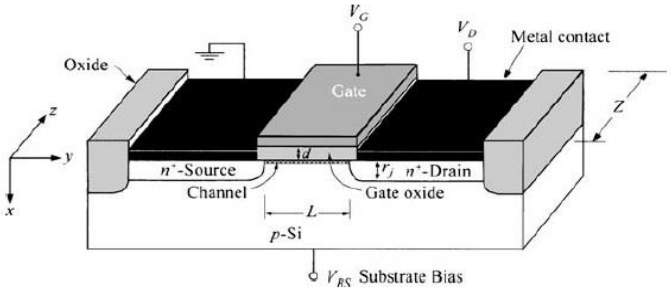

Fig. 1.7 Illustration of schematic of an n-channel MOSFET device. For p-channel device, we substitute the polarity. Image from [11]

With the two ends of the semiconductor are attached to electrodes, this creates two metal semiconductor junctions. When low voltage or ground voltage is applied to the gate, the main channel is shut, however, when a sufficient potential is applied onto the gate, a channel is formed between the two p^- junctions and the source and drain are connected which a large current can flow.

IV. Project Outline

In this project we obtain GeSe nanostructures using VCR technique, which includes a parameter optimization of growing conditions for desired morphology. Subsequently, we will characterize the structures and fabricate optoelectronic devices using suitable samples of GeSe nanostructures to study how the electronic properties of these low dimension nanostructures change when light is shone on the device.

Primary characterization methods include Raman Spectroscopy to study the phonon vibration of the nanostructures, Scanning Electron Microscope to study the morphology of the nanostructures, Atomic Force Microscope to characterize the thickness of the sample, and UV-Vis spectroscopy to study the study the band gap structures of the structures obtained.

After which, we attempt to fabricate the nanostructures into MOSFET devices and test the electronic and optoelectronic performance of the device.

2. Experimentation

I. Sample Preparation:

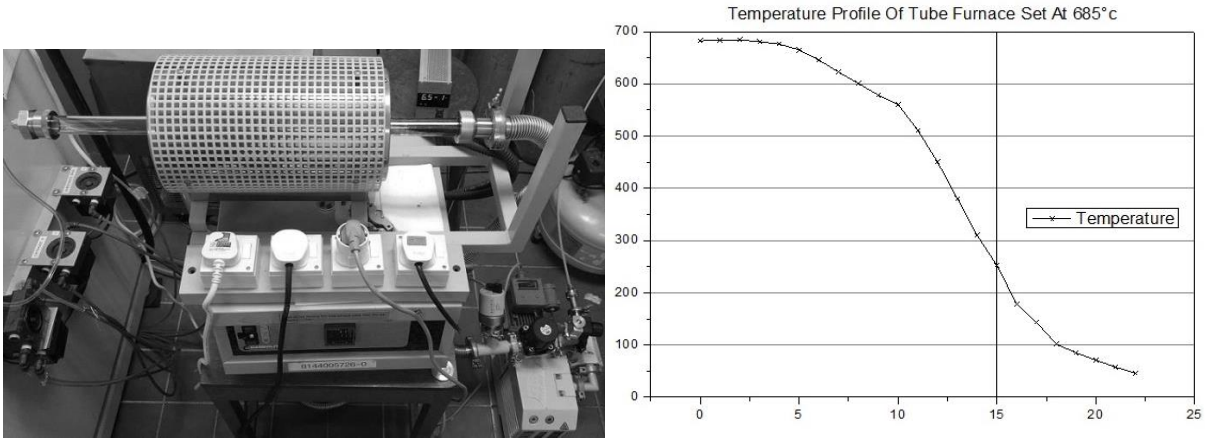

Fig 2.1a Furnace System Used and the 2.2b temperature profile of the tube furnace. The furnace edge is marked at 15cm.

To ensure high purity samples. After the samples are loaded, the tube is first evacuated to a low base pressure of around $3x10^{-2}$ torr, and flowed with Argon gas for 1 minute before turning on the furnace. In the synthesis of nanostructures, depending on the conditions in the tube furnace, the gas molecules could cool down to form crystals of different morphologies. We note that our synthesis process, the variables we could adjust include the amount of substance used, carrier gas and gas flow, temperature of the furnace, pressure in the furnace and the placement of the substrates.

We took the temperature profile of the tube furnace (Fig. 2.1b). The furnace edge is at 15cm. We note that at the center of the furnace, the temperature remains relatively constant. This allows us to have some variance in the position of the placement of the precursor. However, the temperature profile drops significantly from 5cm downstream onwards. The placement of the substrate would significantly affect the surface temperature.

After around 30 attempts, we found that for GeSe nanostructures preparation was most optimal when using a compact tube furnace through a two-step process. We first mix the Ge (−100 mesh, ≥99.999% metals basis, Alfa Aesar) and Se (powder, −100 mesh, ≥99.5% trace metals basis, Sigma Aldrich) in a 1:1 molar ratio and the mixture ground in a crucible for 30 minutes. The powder was then placed on a ceramic boat and inserted into the tube furnace which is then subsequently vacuumed to a base pressure of $3x10^{-2}$ Torr. Argon gas was flowed through the furnace at 200 standard cubic centimeters per minute (sccm). The powder was heated to a temperature of 480°C at a rate of 1°C a minute and kept at that

temperature for 4 hours. The furnace was then left to cool back to room temperature naturally. This powder is then collected.

For the second step of the process, whilst the synthesis process has been successfully carried before using a closed end tube furnace system [4], we use a different layout (Fig. 2.2), which might allow for higher yield or nanostructures with more desirable qualities.

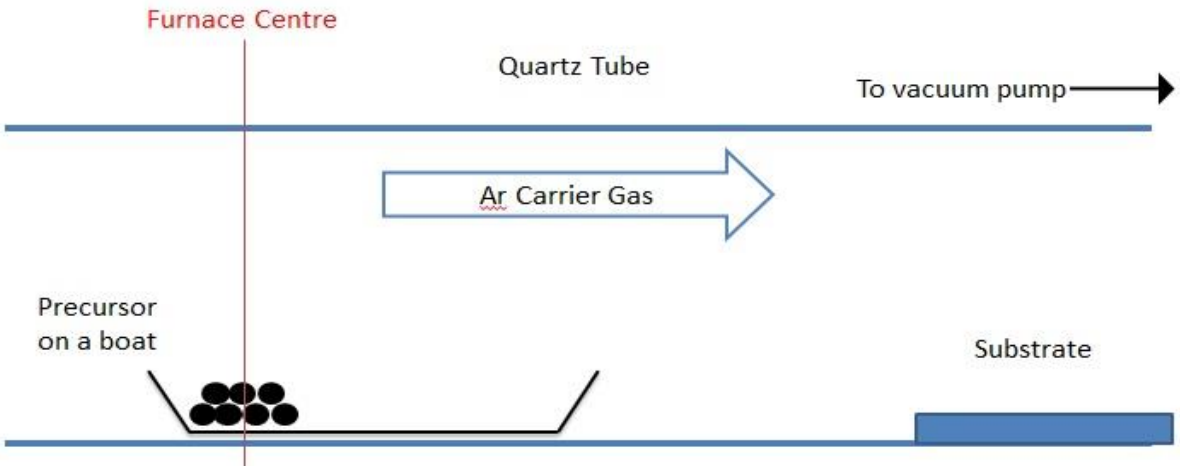

Fig. 2.2 Schematic of Furnace System

In the second step of the process, we used around 20mg of this sintered powder placed in a ceramic boat and aligned to the center of the tube furnace. Si substrate (~ 1cmx1.25cm) is placed 10cm to 20cm down the tube from the powder, with the polished surface facing upwards. The tube furnace is once again vacuumed to a base pressure of $3x10^{-2}$ Torr. We flow 100 sccm of Argon gas through the tube at 0.8 Torr. The furnace is heated from room temperature at a rate of 30°c/min to a temperature of 685°c and kept at that temperature for 40 min. After that, the furnace was left to cool to room temperature naturally. After obtaining the samples, we transfer some structures onto a Si substrate with 300nm wet thermal oxide to prepare for device fabrication.

II. Characterization

Characterization is an important step to ensure what we have synthesized is indeed GeSe nanostructures. In our synthesis process it could be the case that impurities may leak into the furnace to react with the precursor or that Ge and Se compounds of different stoichiometry may form. (Fig. 2.3) We thus carry out characterization in order to ensure that the samples obtained are indeed GeSe samples in the α-phase are obtained.

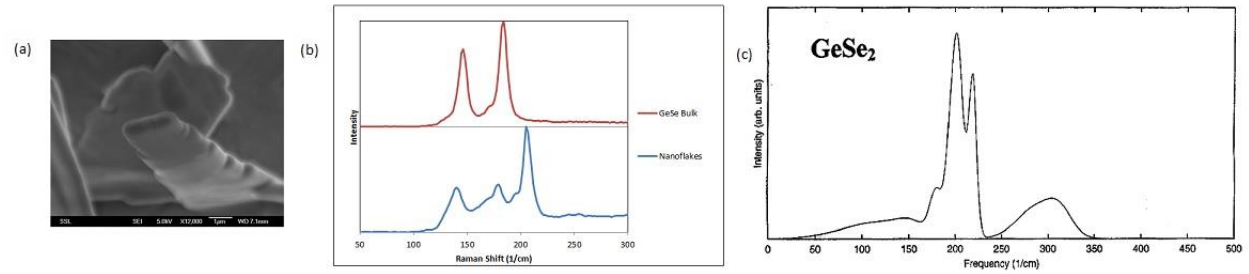

Fig. 2.3 Whilst optimizing growth parameters, one of the prodcuts formed showed Raman peaks that did not belong to α-phase GeSe. We see from analysis that it was the presence of $GeSe_2$ that was in the same lattice as some of the GeSe nanostructures.

1. Raman Spectroscopy

When light is incident on a sample, most of the scattered light is scattered elastically which would result in scattered light having the same angular frequency. This is known as Rayleigh scattering. However, due to inelastic scattering, some of this scattered light would have shifted angular frequency. By measuring the shift in wavelength, we can characterize the molecular vibrations due to the chemical structures in the sample. For the project's purposes, we use Raman spectroscopy for confirmation that the nanostructure samples are of the desired chemical composition. To carry out Raman spectroscopy, the desired spot for carrying out analysis is first determined using a microscope. During analysis, a laser is shone onto a sample. The scattered light is then collected and passed through a monochromator which isolates a single frequency of light and measurements of the intensity of the light of that frequency is taken. This information is then sent to the computer. [12]

Fig. 2.4 Photo of the Raman Spectroscopy Set-Up

All Raman spectroscopy measurements were done using a Renishaw inVia Raman Microscope. (Fig. 2.4) Five runs of measurement were made using 532nm green laser, spot size ~2µm, with the sample exposed for 20 seconds, at the same laser power (~1mW). The monochromator uses 1800 l/mm grating. Repeated measurements at low laser power allow us to see clear distinct peaks [13] without using too much laser power which might cause

sample degradation. For a control, we also measure the Raman spectra of a bulk sample of a high purity GeSe sample (HQ Graphene, purity > 99.995%). We calibrate the Raman Spectroscopy results using the 520cm^{-1} peak of Silicon.

2. Scanning Electron Microscope (SEM)

Under normal microscopes, we are unable to get a good resolution of the nanostructures obtained due to problems like a small depth of focus, due to the short working distance of the microscopes, and insufficient resolution. Thus to properly study to morphology of the nanostructures grown, we used a SEM. The advantage SEM gives us over a conventional optical microscope is the ability to achieve much higher resolution for studying smaller features due to the smaller wavelengths of electrons.

The construction of an SEM is similar to that of an optical microscope. (Fig. 2.5) Whilst a conventional optical microscope uses lenses to manipulate light to focus light onto a point, the SEM uses magnetic fields as lenses to focus an electron beam onto a single spot. The magnetic fields are generated by electromagnetic lenses which are electrical windings around an iron core.

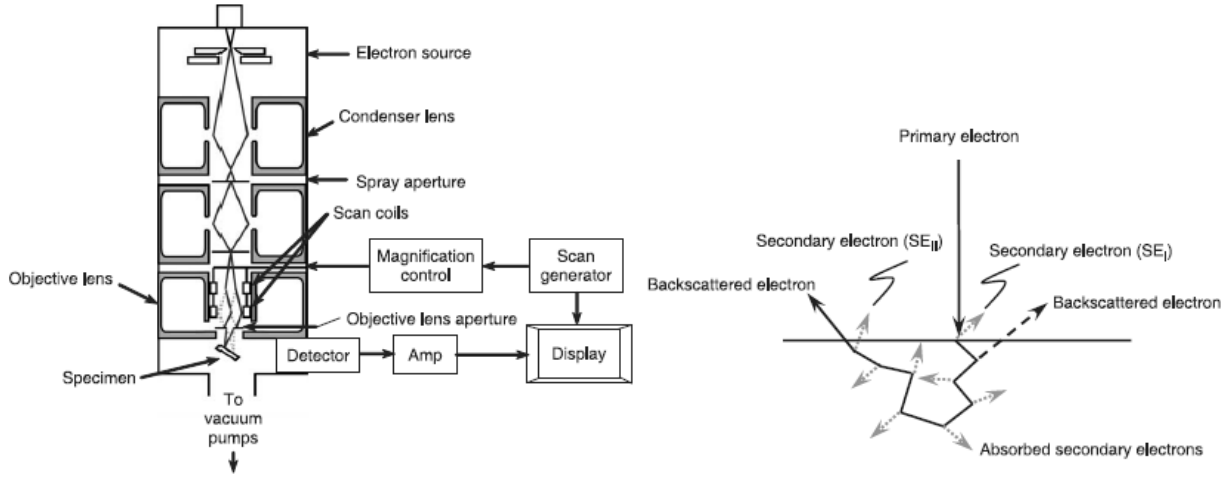

Fig. 2.5a Schematic of SEM and Fig.2.5b Illustration of secondary and backscattered electrons for SEM. Images from [13]

When the focused electron beam becomes incident on the sample, an array of particles and radiation is emitted from the sample. For SEM, the principle particles that are detected are the backscattered electrons and secondary electrons. Backscattered electrons are electrons that are electrons from the electron beam in which their trajectories result in being ejected from the sample surface, and secondary electrons are loose valence electrons that have undergone excitations and have been emitted from the sample surface. As the electron beam scans in a raster pattern, the position of the beam and the detected electrons are processed to form an image. [13]

3. Atomic Force Microscopy (AFM)

We want to get an accurate physical description of the nanostructures we fabricate our devices with. Thus after transferring samples onto a separate substrate, to double check the dimensions of the nanostructures we would be building our devices from, we carry out AFM measurements on them.

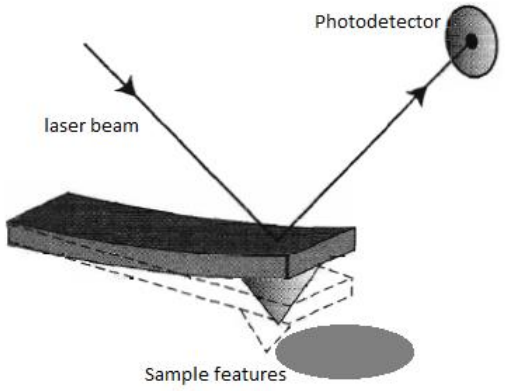

Fig. 2.6 Schematic of AFM. Image Edited from [5]

The AFM does not work by optical principles. Instead, an AFM forms an image by 'tapping' a probe attached to a cantilever onto a surface. As the probe tip taps the surface of the sample under study, forces exerted on the tapping probe by the sample surface as the probe taps the sample causes the cantilever to deflect. The deflection is measured by shinning a laser onto the top of the cantilever and using photo sensors to measure the deflection. By mapping the deflection of the cantilever as the probe taps in a scanning pattern on the surface, the dimensions of the nanostructures can be determined. [5]

4. UV-Vis Spectroscopy

UV-Vis spectroscopy refers to the absorption spectroscopy of Ultra-Violet (UV) and visible light (Vis) of the sample. When photons are incident on a material, if the photon higher than the band gap energy, it could excite an electron from the valence band into the conduction band by the photon radiated. We can describe the energy change of a quantized system by

$$\Delta E = h\nu = hc/\lambda = E_{ph}$$

Where ν refers to the frequency of the electromagnetic radiation, c is the speed of light in vacuum and λ is the vacuum wavelength of the photon. By radiating light onto the surface of the material and observing how much of each wavelength of light is absorbed, we obtain different kinds of information about the material. In the UV-Vis range (~200nm to 350nm), the absorption spectroscopy can be used to obtain information such as electronic

transitions within d-orbitals of transition metal ions, defects, or in this case band gap transitions between the valance and the conduction bands. [14]

To determine the band gap from the spectroscopy results, we use a technique called the Tauc Plot. From the Tauc, Davis Mott relation given by

$$(h\nu\alpha)^{1/n} = B(E_{ph} - E_g)$$

Where h is the Planck's constant, ν is the frequency of vibration, α is the absorption coefficient, E_g is the band gap, n is 1/2, 3/2, 2 or 3 dependent on the type of bandgap, and B is the proportional constant. For an indirect bandgap such as the sample we are studying, we use n value of 2.

Where R_∞ refers to the reflectance at infinite thickness of the sample and s refers to the scattering coefficient. This can be rewritten as $(E_{ph}F(R_\infty))^{1/n} = B(E_{ph} - E_g)$ using the Kubelka-Munk function. Should we plot the obtained spectrum expressed in the Kubelka-Munk function given by,

$$\mathrm{F(R_\infty)} = \alpha/\mathrm{s}$$

If we extrapolate the straight line portion of the absorbance spectra to α = 0, we can determine the band gap of the sample. [15]

The UV-Vis spectroscopy set up (see Fig. 2.7) includes a lamps source, which passes through a monochromator. The light is targeted onto the sample through a microscope and subsequently passed through to a detector. We transferred some samples onto a quartz substrate. Three readings were recorded, once in the dark without the lamp, once with the light directed at the nanostructure and once on the quartz substrate beside the sample. By comparing the resultant spectra, we are able to determine the UV spectroscopy of the nanostructures. The Schematic is illustrated below.

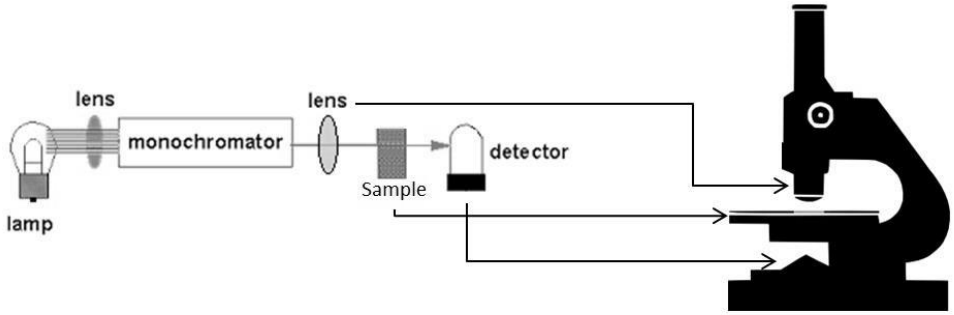

Fig. 2.7 Schematic of UV-Vis Spectroscopy

III. Device fabrication

To build our device, the nanostructures, we used photolithography to etch out electrodes across the nanowires and nanoflakes. We choose to carry out experimentation on these nanostructures as there is not much literature on the performance of GeSe nanowires and nanoflakes as of the time of experimentation.

To do that, we transferred the nanostructures, from the Si substrate that it was grown on, onto a silicon substrate with 300nm wet thermal oxide via contact. Three drops of positive photoresist solution (AZ1518) was dropped onto the substrate and spun in a spinner for one minute at 4000rpm. The sample was then heated over a heater at 100°c for one minute. We then placed the samples in the laser writer and exposed the samples to the 400nm laser at 1.35mW. We do not use a high powered laser as we only need to expose the photoresist to some light. Too much laser power could result in poorer resolution in the exposed prints onto the photoresist, or burning away of the sample. Once the prints of the template for the electrodes were exposed, the samples were placed in a developer solution (KOH and potassium borate buffer solution) for around one minute. This would result in photoresist exposed to the laser being washed away, leaving empty areas of the silicon substrate.

We then use thermal evaporation to etch 5nm of chromium and 100nm of gold onto the substrate to form the electrodes. Subsequently the samples are washed with Acetone to remove the remaining photoresist, which leaves only the etched electrodes on the substrate. Subsequently, the sample is attached a chip holder and the electrodes are wire bonded onto the connectors of the chip holder. To add a gate, either the thermal oxide on the substrate was scratched away and a wire was bonded directly onto the Si substrate or a wire was bonded to the chip holder which is connected to the substrate.

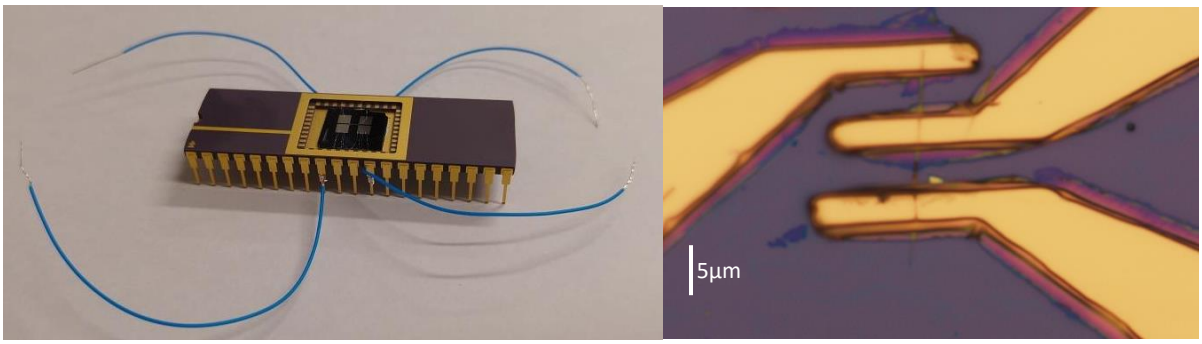

Fig. 2.8 Resultant device attached to chip holder with wires attached for performance testing. Picture of one of the devices fabricated and tested

IV. Device Testing

Several parameters of the device were tested to evaluate the devices performance. To test the device, we use a source meter unit (Keithley 6430).

1. IV Characteristic

We test the I-V characteristics of these devices as a MOSFET device to see how these devices perform as normal semiconductors and how the performance of the device changes as a gate voltage is applied. We set the gate voltage at a constant and sweep the source voltage. Subsequently, we will hold the source voltage constant and sweep the source voltage to understand how current changes along changes in gate voltage.

2. Photocurrent

Subsequently, we test for the presence of photocurrent. To do this, we compare the IV characteristic of the nanowire under dark conditions and when radiate the nanowire with a focused laser beam system (532nm) set at varying values of power to shine onto the device.

3. Photoresponse

The third test measures the response time between the laser exposed states and dark states, and also gives us confirmation of the changes in the current when the sample is exposed to a laser. To do this, we place a shutter before the laser. A constant voltage is applied across the nanowire, after 5 seconds, the shutter is opened and the laser will radiate onto the nanowire. After radiating the nanowire for 5 seconds we shut the shutter. We then vary the power of the laser to see if this laser response changes with different laser powers.

We will then evaluate the performance of these devices using several parameters that will be discussed later.

3. Results and Discussion

I. Synthesis

For the parameters used to synthesize the nanoparticles, we report that growth of the nanostructures occur around in the region around 12.5cm to 15cm (250°c to 410°c) downstream from the center of the furnace where the precursor powder is. In colder regions, only a thin film of GeSe is deposited. The temperature range is in agreement with other attempts to synthesize GeSe nanomaterials. [4, 9] Synthesis of nanostructures occurs at both at the top polished surface and the bottom unpolished surface of the SiO_2 substrates. Different nanostructures have been synthesized including nanoribbons, nanowires and Nanoflakes. In our synthesis, only nanowire growth occurs at the top polished surface whilst nanoribbons and nanoflakes and nanoribbons have been observed to be growing at the bottom unpolished surface. (Fig. 3.2)

We also observe that there is a much higher density of nanostructures at the side of the substrate nearer to the furnace. This could be due to a higher surface temperature of that side of the substrate. [8] We also note that larger nanostructures occur more at the bottom surface of the substrate. On the bottom surface, the sizes of the nanoparticles decrease as we move downstream.

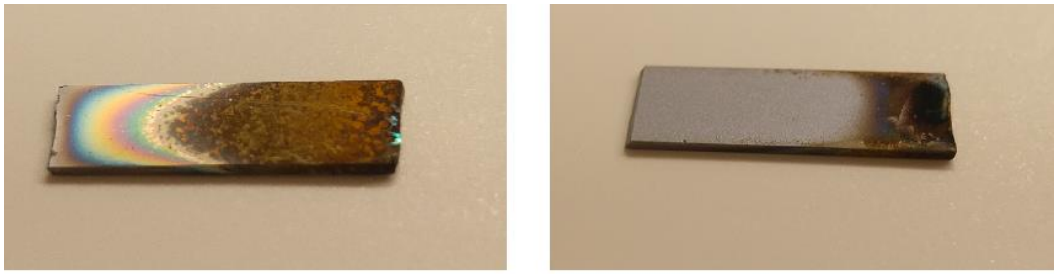

Fig. 3.1 Photo of resultant Si substrate with synthesized nanostructures. The right side of the substrate was nearer to furnace center. (a) Smooth surface of substrate facing upwards and (b) Rough surface of substrate facing downwards. Substrate was placed around 12.5cm to 13.75cm from furnace center (410°c - 325°c)

To explain this phenomenon, we propose that if GeSe has a similar growth mechanism as GeS, which has similar lattice structure [2], then having larger nanostructures at the bottom surface could be due to the diffusion of GeSe being much higher at the bottom of the substrate. [8]

A possible scenario is that the molecules are being trapped in regions between the substrates and underneath the substrates, resulting in higher density of molecules in those regions. Having a higher density of GeSe molecules in those regions, there would be higher

collision rates, resulting in growth of larger nanostructures. After larger structures are formed, there would be a lower concentration of GeSe nanoparticles to be carried downstream by the Argon gas in those regions. This could explain why the structures reduce in size as we move downstream.

It was observed during the measurement of the temperature profile of the furnace that the furnace center temperature fluctuates by about ±5°c. This might be a reason that it growth of GeSe nanostructures were not consistent.

II. Characterization

1. SEM

Studying the samples under microscope, we were able to observe the morphologies of the nanostructures in greater detail.

The nanoflakes synthesized that were observed have a thickness of about 200nm while the width of the flakes varies greatly. We see that the edges of the flakes are not smooth but are in fact uneven.

We notice from studying the nanowires that the nanowires branch off from flakes of GeSe. The nanowires all have a diameter of ~200nm and seem to become thinner close to the tip. The nanowires also can grow up to 15µm in length. It has been proposed that the growth of the branching off the flake into nanowires could be explained by valley shaped defects at the edge of the nanoflakes. [9] This can be further supported by the uneven edges of the nanoflakes obtained and the similarity between the thickness of the Nanoflakes and the diameter of the nanowires.

The nanoribbons that have been obtained also measure about 200nm. We observe that sometimes, ribbons branch off from a single nucleation site, arranging the ribbons into a flower like arrangement. (Fig. 3.2 (c)) If we study the morphology of the nanostructures synthesized on the bottom surface of the substrate, we can see that it appears many of the nanostructures appear to be branching outwards. This gives support to that the growth mechanism employed here is indeed a VCR process.

We also observe that on the surface of the GeSe flakes there is unevenness and there appears to be spots. This might suggest that the flakes do not have a very high crystallinity as compared to the ribbons and the wires, possibly due to the higher growth rates of the nanoflakes.

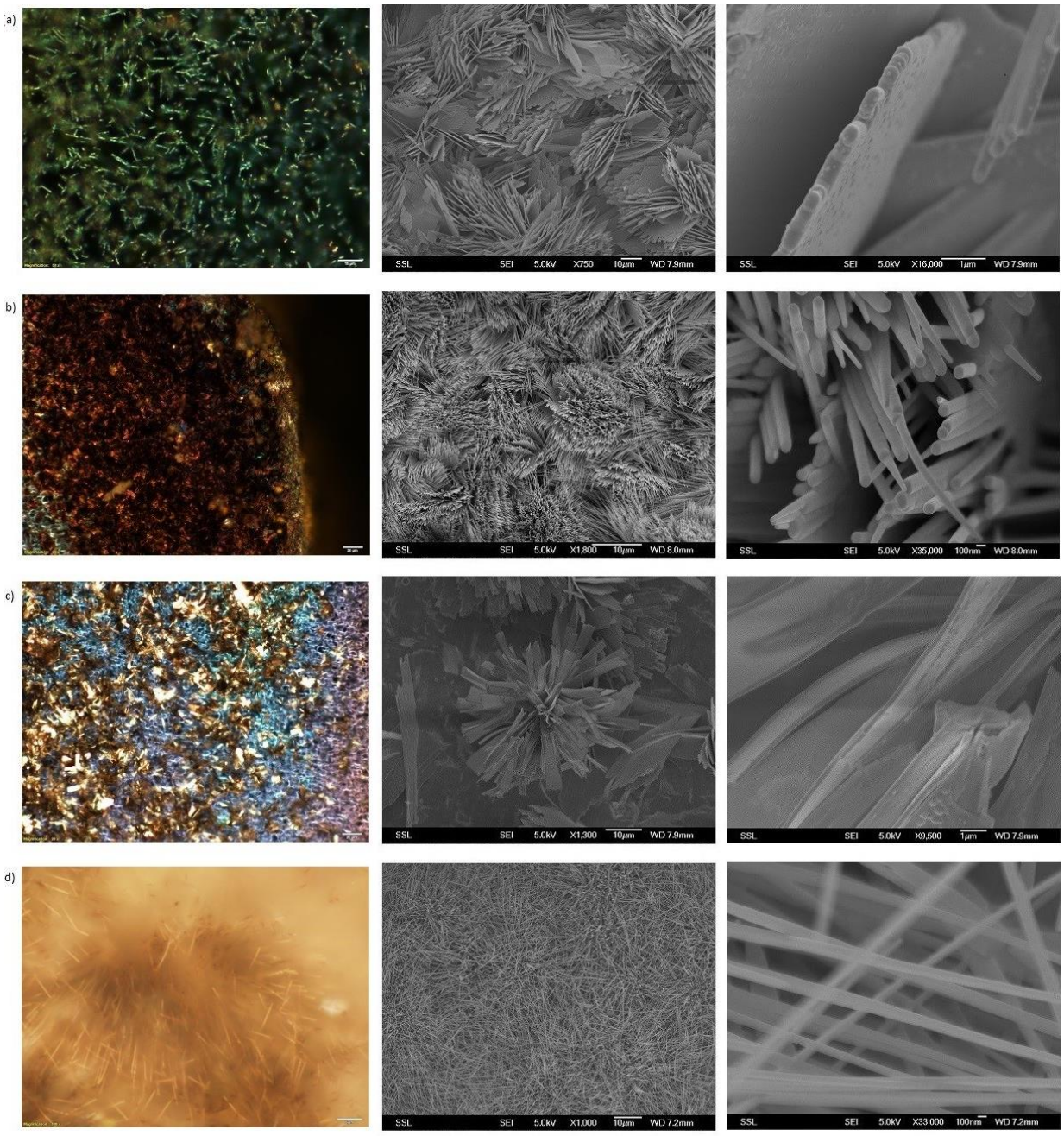

Fig 3.2 Microscopy and SEM images of (a) Nanoflakes at bottom surface of substrate (b) Nano wires at bottom surface of substrate (c) Nano ribbons at bottom surface of substrate and (d) Nanowires at top surface of substrate. Pictures placed at the top show structures at lower magnification whilst images at bottom show the same area under increased magnification.

2. Raman Spectroscopy

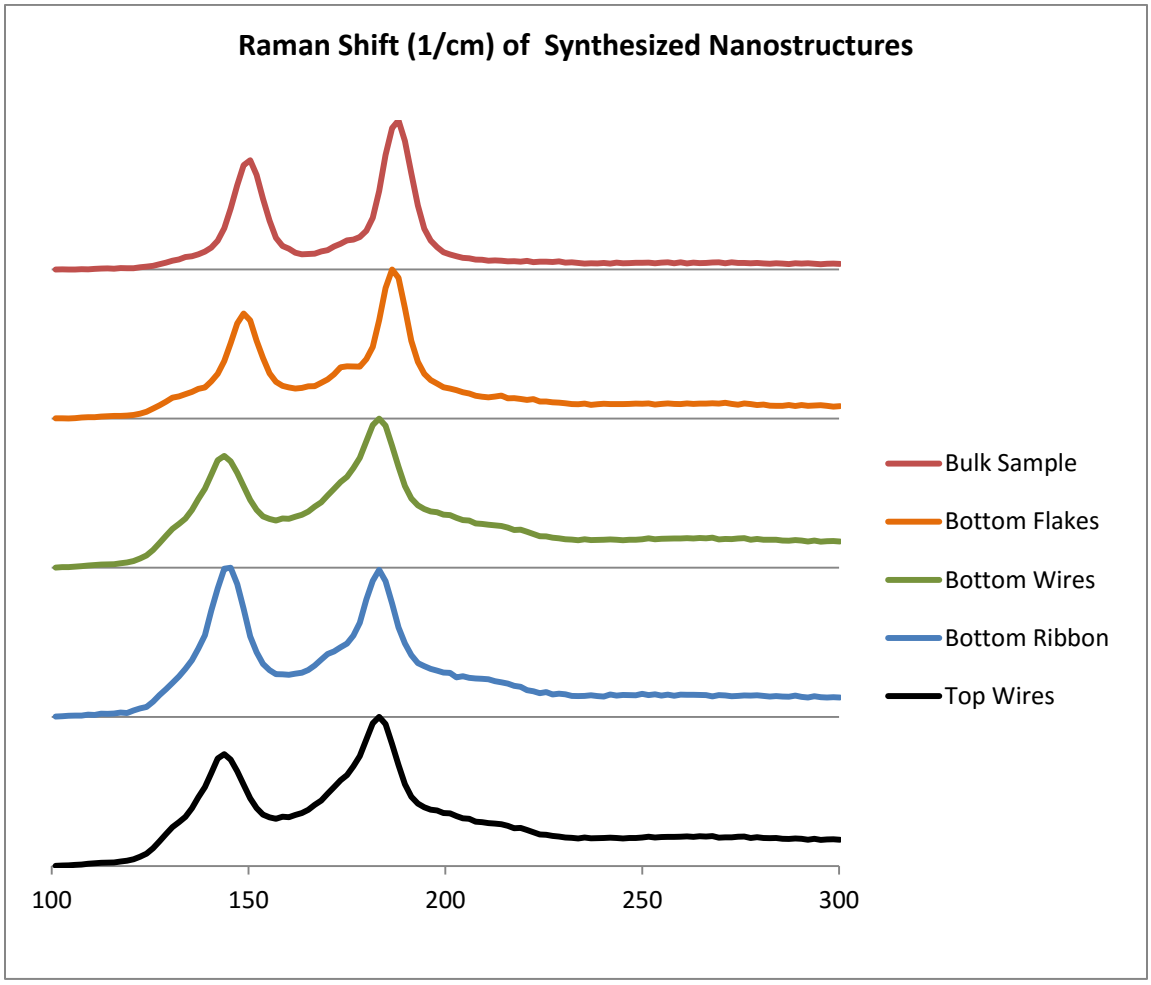

Fig. 3.3 Normalized Raman Spectroscopy of Different GeSe Nanostructures

The Raman spectroscopy of the different samples showed that all the different morphologies obtained at the optimized parameters are indeed GeSe nanostructures with similar lattice as the bulk sample. (Refer to Fig. 3.3) We observe that in the spectra of bulk GeSe obtained, we get two strong peaks at 150cm^{-1} and 188cm^{-1}. These Raman peaks can be attributed to the transverse optical modes in the B_{2u} and A_g modes respectively. There is also a peak that can be seen at 175cm^{-1}. This is due to the transverse optical mode B_{1u} mode. [16] From this, we can conclude that the nanostructures we have synthesized in the lab are indeed GeSe nanostructures.

In the Raman spectra of the synthesized nanostructures, the peaks observed are similar. However, for the nanostructures, the peaks show less Raman shift. For the Nanoflakes found at the bottom of the Si substrate, the peaks are 2cm^{-1} less than that of the bulk sample. For the nanowires synthesized on both sides of the Si substrate and the

nanoribbons that were synthesized on the bottom of the Si substrate, there is a larger difference of around 5cm^{-1}.

The shift that occurs could be attributed to some factors. It has been shown in other materials that different materials thickness could affect the position of the Raman peaks [8, 17, 18]. Apart from thickness, lattice strain has also shown to contribute towards Raman peak shifts [19].

3. Atomic Force Microscope

For nanowires, from the map that the AFM has produced, we measure along the length the width of the nanowire at several places to understand how the dimensions of the nanowire changes along its length. We analyze the AFM reading by fitting the curves to step functions. We measure height of 164.97±22 and width of 468.7nm for measurement 1 at the tip of the nanowire, height of 242.41nm and width of 312.8nm for measurement 2 in the middle of the nanowire and height of 227.4nm and width of 312.8nm for measurement 3 near the base of the nanowire. (see Fig. 3.4a)

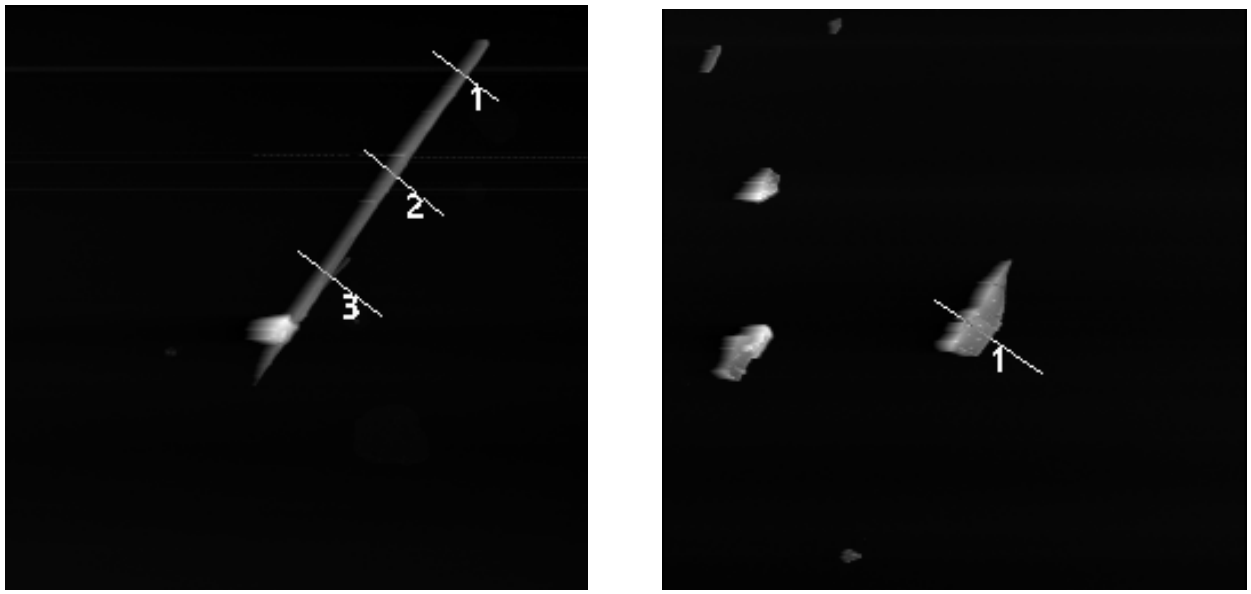

Fig. 3.4a Sites where measurements were taken from a nanowire sample and 3.4b one of the measurements where the AFM map was sampled for thickness measurement.

For the nanoflakes, after approximating the data to step functions, we measured an average height of 243.86nm for the Nanoflakes. These measurements are in agreement with the data we obtained from the SEM images.

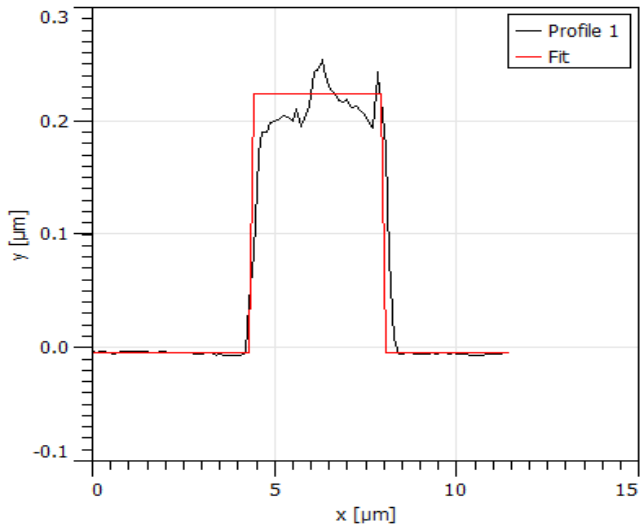

Fig. 3.5 Fitting to step function performed for one of the flake thickness measurements

One interesting thing to note is that at one end of the nanowire measured there is a stub. This further supports the idea that the nanowires branched off from nucleation sites. This gives support to the VCR growth mechanism proposed.

4. UV-Vis Spectroscopy

The absorption spectroscopy of the samples was obtained. (Fig. 3.6) To determine the band gap of the sample, the data for straight line portion of the $\alpha^{1/2}$ curve was obtained and fit into a linear plot using linear least squares regression.

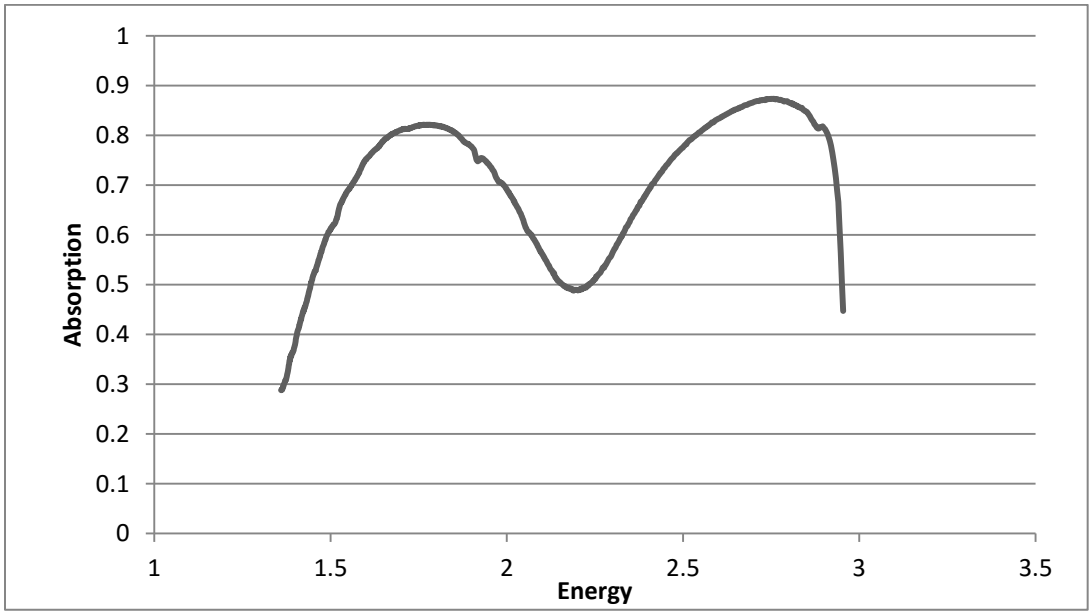

Fig. 3.6 Absorption spectra of sample

From the results obtained the band gap was calculated to be 1.08±0.02eV. This gives a discrepancy of 4.6%. We can say with certainty that our sample indeed has the bandgap of GeSe. However, we observe a drop in the absorption from 1.75eV to 2.75eV. This might be caused by impurities or dust. Furthermore, as the absorption spectrum is not complete, the line fitting was only done onto a small part of the data. For greater certainty, we would need to do collect more spectra for analysis.

III. Device Fabrication and Testing

In our measurements of the performance of GeSe devices we measured 2 types of Nanostructures, both of which are GeSe nanowires. Attempts to measure other morphologies such as flakes did not turn out successful as the nanostructures got washed away along with the acetone when carrying out lithography.

This could be due to the flakes being too big in size. When studying the nanoparticles under SEM and AFM, we saw that for most of the flakes and the ribbon structures obtained, there is evidence that structures stem out from a single nucleation point. If the flakes were transferred together onto the substrate still attached onto other flakes, the particle size would be quite big.

The forces that hold the particle onto the substrate is likely to be only Van Der Waals forces. When the size of the structure is too big, the Van Der Waals forces that hold the structure on to the substrate might not be sufficient resulting in the nanostructures being easily washed away.

Unfortunately, almost all the devices fabricated by the nanowires we synthesized failed. Most measurements taken show the IV curve of the devices to be in the same order of magnitude as that background current, where the term ‘background’ current here refers to current measured when the source meter unit is not attached to a device. It may be the case that most of the devices have an IV characteristic that is smaller than the precision allowed by the source meter unit.

If the failure of the device is due to GeSe structure, failure can be attributed to factors such as crystal defects, cracks, surface contamination, and junction deterioration amongst other reasons [20]. Considering that the nanowires are very thin, breakage and defects might be very common especially so during the transfer process.

1. IV Characteristic

We managed to get GeSe nanowire samples that were prepared using similar synthesis methods, and shall discuss the performance of these materials instead. Of the samples

obtained, one was a thicker wire (~1000 nm diameter) than the other (~ 200 nm diameter). Both devices have a similar distance between the electrodes. (~ 5µm)

The IV curve of the GeSe nanowires obtained is shown below

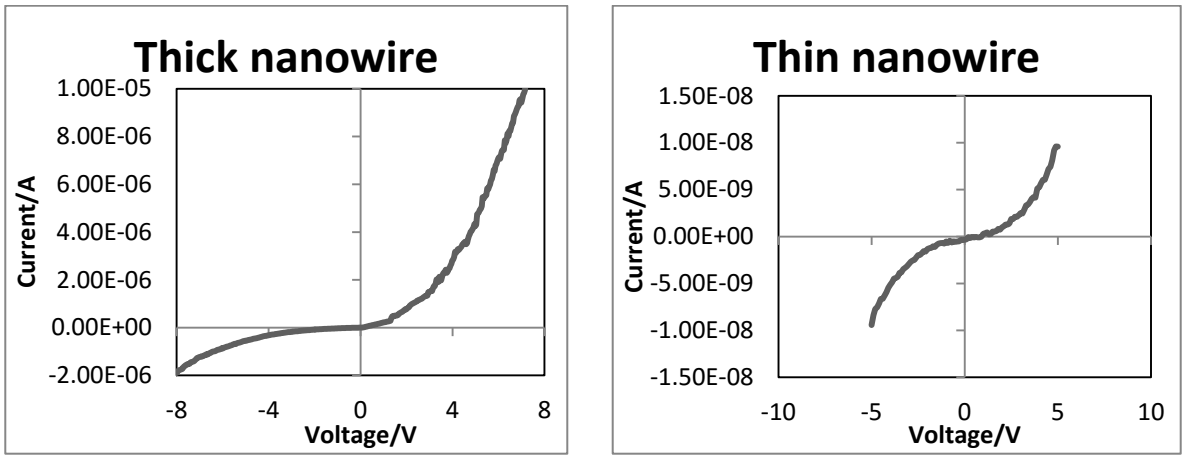

Fig. 3.7 GeSe nanowires tested and corresponding IV curve in a dark room

We observe that the thicker sample has a higher conductivity than the thinner sample. Both samples have the IV characteristic of a p-n junction. We see that the thinner nanowire has a resistance of 2 orders of magnitude higher than the thicker wire.

The thinner wire subsequently failed and only the thicker wire was tested on for photocurrent.

2. Photocurrent

We tested for photocurrent of the wire using a 532nm laser set at 0.750mW, 0.531mW and 0.275mW. The laser power was measured using a laser power meter. The results are shown below. (Fig. 3.8) We observe that the sample tested has very little photocurrent. The photocurrent is most noticeable when observing IV curve at where potential applied to the nanowire is at 10 V.

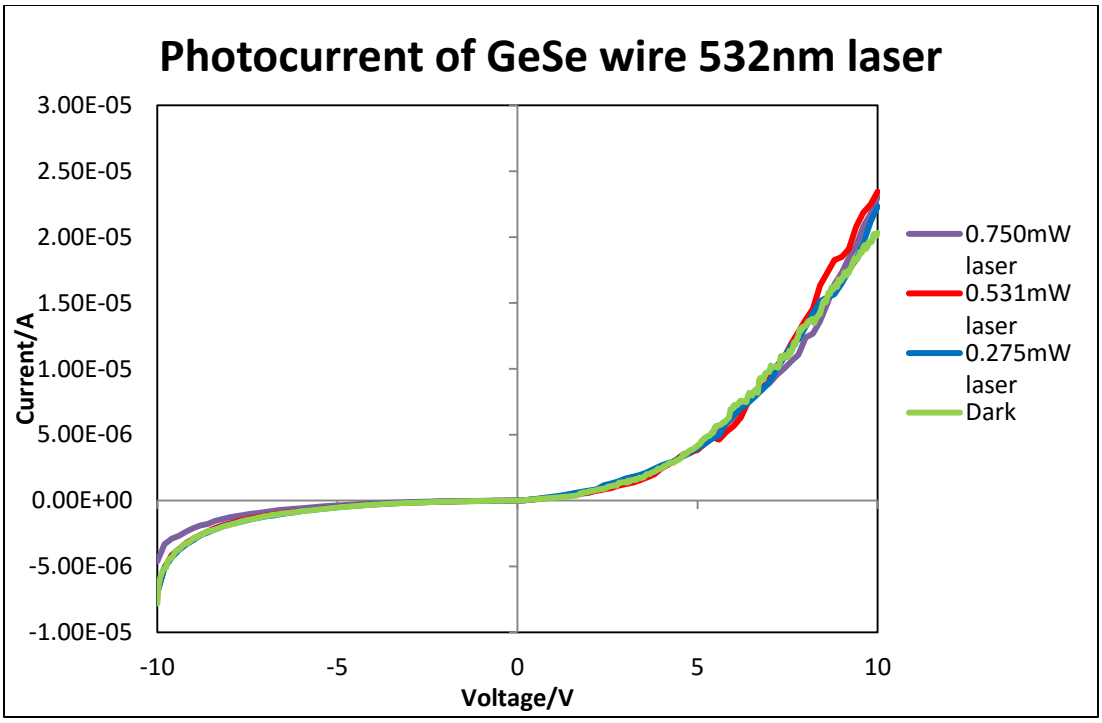

Fig. 3.8 Photocurrent of GeSe at different laser power

3. Photoresponse

As the photocurrent is so small, to better observe the change in the current when the sample is exposed to a laser as compared to when the sample is not exposed. This also gives us a picture of how fast GeSe photocurrent responds to the laser exposure. We for this test, we set potential across the wire at 10V. (Fig. 3.9)

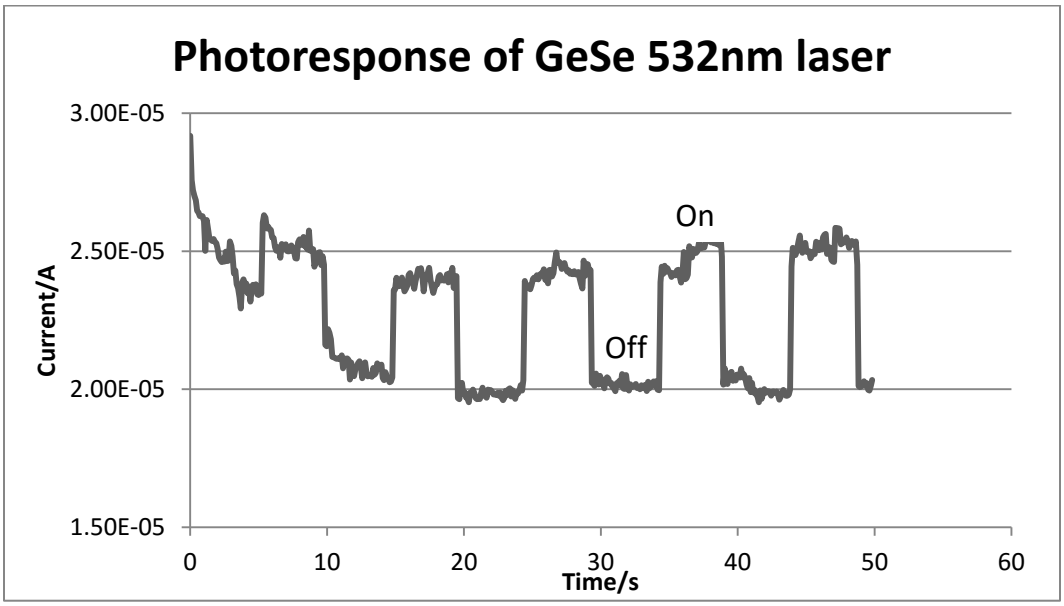

Fig. 3.9 Photoresponse of GeSe wire using 532nm laser

We can now see clearly the photoresponse of GeSe. We can also see that there is a drop in the current as time passes. To ensure that this is not due to the laser changing the properties of the wire, the measurement was repeated without any laser exposure.

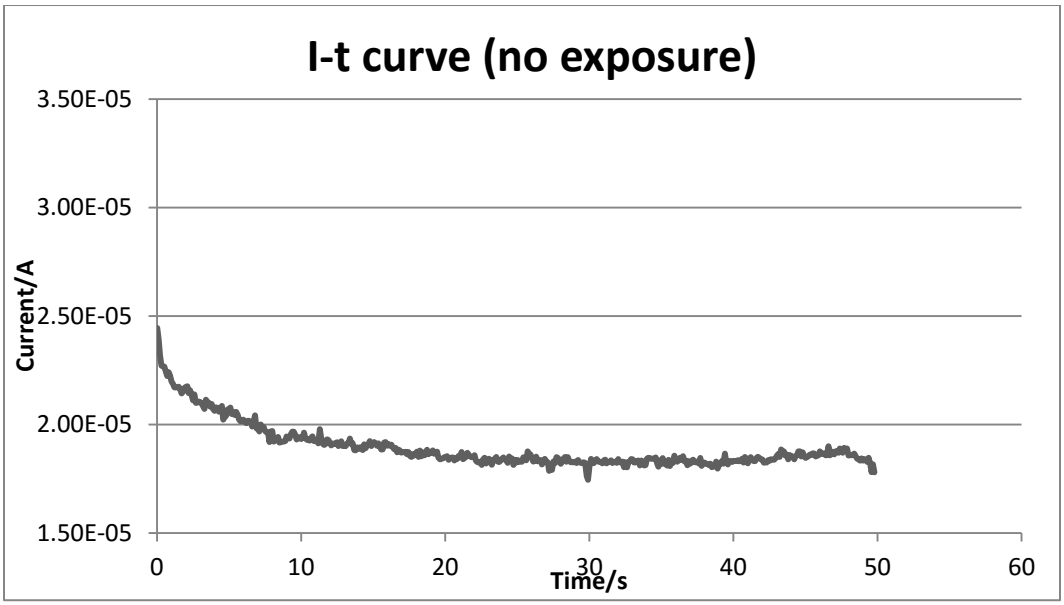

Fig. 3.10 I-t curve of sample without exposure

We can see that the current of the device stabilizes after some time. Therefore, to measure the difference in the photocurrent, we only took measurements when the current reading is stable. We report that under 0.048mW μm^{-2} laser power, we measured 4.55µA; under 0.038mW μm^{-2} laser power we measured 3.68µA; under 0.027mW μm^{-2} laser power we measured 2.84µA.

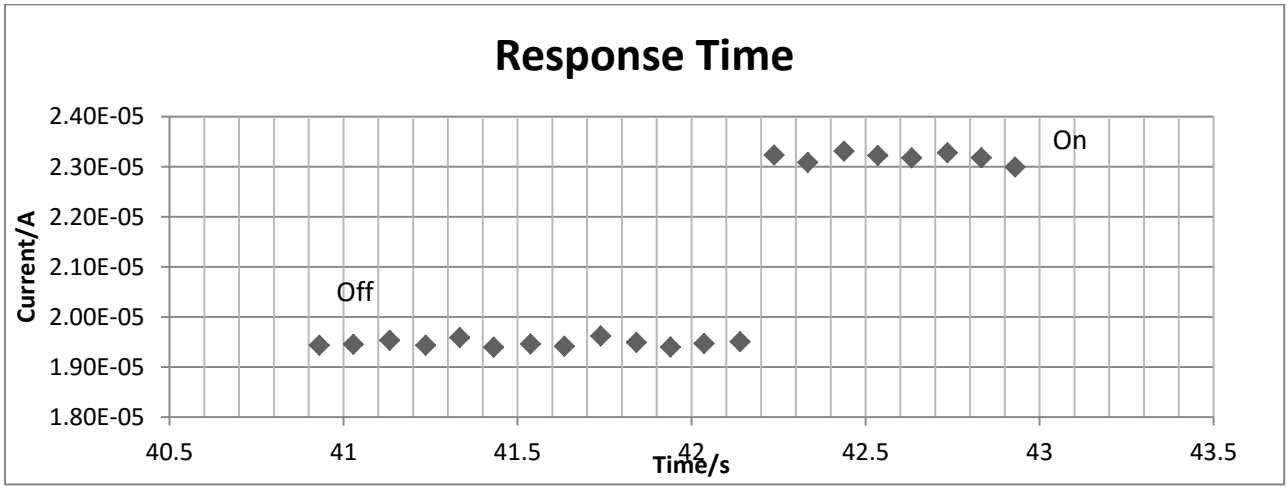

Fig. 3.11 Evaluating response time verticle grid lines are 0.1s apart

From the data we obtained, the response of the device from laser 'off' to 'on' state is less than 0.1s apart. (Fig. 3.11) More experimentation would be needed to increase the precision of the measurement.

4. Evaluation of device

We evaluate optoelectronic devices using some parameters. These shall be discussed below.

a) Photoresponsivity

Photoresponsivity, R_{res}, measures the photocurrent generated by the laser light per unit power in the laser that is incident onto the device. It is given as

$$R_{res} = \frac{I_{pho}}{P_{opt}} = \frac{(I_{illum} - I_{dark})S^{-1}}{P_{inc}}$$

Where P_{opt} is the measure of the power of the laser incident on the nanomaterial, I_{pho} is the measure of the photocurrent, and S is the irradiated area of the optoelectronic device. [1, 21]

To measure photocurrent, we took the difference in average of the laser 'on' and 'off' values. We calculate using a radiated area of 2 μm^2 and laser powers of 0.048mW μm^{-2}, 0.027mW μm^{-2} and 0.038mW μm^{-2} we report R_{res} to be of an average of 12.3 mA W^{-1} under 532nm laser at 10 V potential.

b) External Quantum Efficiency

External Quantum Efficiency, EQE, measures the number of electrons detected per incident photon. It is given as

$$EQE = \frac{hcR_{res}}{e\lambda}$$

Where h is Planck's constant; c is the speed of light, e is electron charge and λ refers to the excitation wavelength of the light. [1, 21]

We report the EQE of the GeSe nanowires to have an average of EQE of 70.2%.

c) Specific Detectivity

Another parameter used to evaluate the nanostructures is specific detectivity which a key figure-of-merits. It is given by [1, 22]

$$D^* = \frac{R_{res}S^{\frac{1}{2}}}{(2eI_{dark})^{\frac{1}{2}}}$$

We report a D* value for GeSe nanowires to be 3.81 x 10^9 Jones.

To get a sense of the performance of GeSe as compared to other materials and morphologies, we can compare these parameters measured on GeSe nanowires as compared to some other materials.

Photodetectors	R_{res} (A W^{-1})	EQE (%)	Reference
GaS nanosheet	4.2	2050	[23]
Single Layer MoS_2	7.5 x 10^{-3}		[24]
Solution Synthesized GeSe	173	5.32 x 10^4	[1]
Few Layer GeSe	3.5	537	[4]
GeSe Wires	12.3 x 10^{-3}	70.2	This Work

Table 3.1 Comparison of some of the parameters with other materials

From the comparison of values, it appears that the performance of GeSe is comparable to Single Layer MoS_2 very well as a photodetector for 532nm laser.

4. Conclusion

I. Report Summary

In this project, we synthesized different types of GeSe nanostructures on Si substrate using a vapour deposition process. This was done by optimizing the yield of GeSe nanostructure growth by altering growth parameters such as the temperature, pressure, the amount of precursor used, gas flow rate and the placement of the substrate.

Subsequently, the synthesized nanostructures were characterized. We used Raman spectroscopy to identify the synthesized nanostructures and identified them as α-phase GeSe. We then carried out Scanning Electron Microscope to study the morphology and surface features of the synthesized nanomaterials. We determined the growth mechanism to be a Vaporization Condensation Recrystallization process supported by morphology of the resultant nanostructures. We measured the nanostructures under AFM and found that the nanostructures generally have a thickness of ~200-300nm. We then used UV-Vis absorption spectroscopy to study the band features of the synthesized GeSe and found the band gap to be 1.08±0.02eV which corresponds to 1148nm, which is in agreement with the band gap of earlier measurements of bulk GeSe.

We then went on to attempt to fabricate MOSFET devices using GeSe nanowires and nanoflakes. Device fabrication of nanoflakes failed as the flakes did not stay on top of the substrate. Device fabrication of nanowires was much more successful. However, most of the devices failed during testing. We managed to obtain GeSe wires from similar growth methods. However, we were unable to test these devices as MOSFETs.

Using this wire, we measured the I-V characteristic of GeSe nanowires and the changes to the current when the GeSe wire is radiated with a 532nm laser. The power of the laser was varied and the resultant change in the photocurrent was measured. We then went on to calculate photoresponsivity and the External Quantum Efficiency and determined that the GeSe wire performance is comparable to single layer MoS_2.

5. Further areas of exploration

I. GeSe as MOSFET device

Though we had intention to test the how the nanostructures would perform as a MOSFET device, with the failure of many of the devices, it became difficult to do so within the constraints of time provided for this project. Along with testing GeSe as a MOSFET device, perhaps finding ways to modify the device such as using a high powered laser to react the sample or building a heterojunction to improve its performance might be more meaningful.

II. Materials Synthesis and Sample Preparation

In our analysis of GeSe, we proposed that the growth of GeSe under those conditions is diffusion-limited.(section 2.I)If the growth rate is indeed diffusion limited, we could explore synthesis using a different furnace layout such as using a closed end tube furnace system. This could help to increase the yield of GeSe nanostructures, or give us better control of the GeSe nanostructure synthesis. Furthermore, this would allow us to use less amounts of precursor per growth attempt.

As for the samples we have now, we can use a focused laser beam system to modify the thicker samples to attempt to reduce the thickness of the GeSe structures to observe changes in the optical, electronical and optoelectronical characteristics of the nanostructures before and after laser modification.

Apart from GeSe, there are three other semiconductors in the 'phosphorene analogues' family. For further experimentation, there seems to be a lot of work recently on GeSe and GeS materials and not much recent work, as of the time of experimentation, on Tin Sulfide and Tin Selenide. We could look into the synthesis of nanostructures of Tin Sulfide (SnS) and Tin Selenide (SnSe) using vapor deposition methods to see how well these materials perform as optoelectronic devices.

III. Characterization and Device Fabrication

Over the course of the project, we characterized the synthesized materials to be α-phase GeSe by using Raman spectroscopy. To have a greater certainty of the composition and structure of the materials, we could use X-Ray diffraction (XRD) and Transmission Electron Microscope (TEM) to study the lattice structure and study the crystallinity of the synthesized materials.

We see that in the SEM images of the nanoflakes (Fig. 3.2) we see that the surface of the flakes is not smooth and that there are round protrusions. Also, as discussed earlier, one of the reasons that could explain the failure of the devices was defects and cracks. To properly

understand the reasons for the device failures and the surface morphology of the nanostructures, we could look into carrying out TEM, XRD and SEM experiments. With a better understanding of the cause of the device failures, we might have a better idea of which processes we can look into to increase success rates.

One such process to look into may be the transferring of the nanostructures from one substrate onto another, the wanted substrate 'touches' the surface which the nanomaterials are grown onto. This might put the nanostructures under strain and may be able to introduce cracks to the nanostructure lattice. This might also help us improve the device performance.

IV. Valleytronics and valley-hall effect

It was reported that apart from having a desirable lattice structure for a wide range of applications, the group-IV monochalcogenides have multiple valleys. As phosphorene analogs have a rectangular unit cell, these valleys are situated on the axes of the Brillouin zone. Due to this, as opposed to using circularly polarized light on Transition Metal Dichalcogenides, valley separation can be performed using linearly polarized light. Additionally, the orientation of the valleys allows valley separation using transverse non-linear conductivity. A theoretical calculation was done on Tin (II) sulfide and it was calculated that there would be a transverse current arising in a perpendicular direction. Simply put, it was calculated that when an electric field is applied to the y direction of a sample of Tin Sulfide, should the sample be irradiated by a polarized light source, depending on the polarization of the light, a transverse current can be detected in the z direction. [25] This effect has been well studied in MoS_2 [26, 27] where a circularly polarized light is used to induce a transverse current, but the effect is still not yet experimentally verified upon for the phosphorene analogues.

Bibliography

1. *Solution synthesis of GeS and GeSe nanosheets for high-sensitivity photodetectors.* **Parthiban Ramasamy, Dohyun Kwak, Da-Hye Lim, Hyun-Soo Ra, Jong-Soo Lee.** 2016, Journal of Materials Chemistry C, Vol. 4, pp. 479-485.

2. *Phosphorene analogues: Isoelectronic two-dimensional group-IV monochalcogenides.* **Lidia C. Gomes, A. Carvalho.** 8, s.l. : APS, 2015, Physical Review B, Vol. 92.

3. *Black phosphorus field-effect transistors.* **Likai Li, Yijun Yu, Guo Jun Ye, Qingqin Ge, Xuedong Ou, Hua Wu, Donglai Feng, Xian Hui Chen, Yuanbo Zhang.** 5, 2014, NAture Nanotechnology, Vol. 9, pp. 372-377.

4. *NIR Schottky Photodetectors Based on Individual Single-Crystalline GeSe Nanosheet.* **Bablu Mukherjee, Yongqing Cai, Hui Ru Tan, Yuan Ping Feng, Eng Soon Tok*, and Chorng Haur Sow*.** 2013, ACS Appl. Mater. Interfaces, pp. 9594-9604.

5. **Kittel, Charles.** Introduction To Solid State Physics, 8th Edition. s.l. : John Wiley & Sons, Inc, 2005, pp. 187 - 191.

6. **Neamen, Donald A.** *Semiconductor Physics and Devices: Basic Principles.* New York : McGraw Hill, 2003.

7. *Single-Crystal Colloidal Nanosheets of GeS and GeSe.* **Dimitri D. Vaughn, Romesh J. Patel, Michael A. Hickner, Raymond E. Schaak.** 43, 2010, J. Am. Chem. Soc., Vol. 132, pp. 15170-15172.

8. *Role of Boundary Layer Diffusion in Vapor Deposition Growth of Chalcogenide Nanosheets: The Case of GeS.* **Chun Li, Liang Huang, Gayatri Pongur Snigdha, Yifei Yu and Linyou Cao.** 2012, Acs Nano, pp. 8868 - 8877.

9. **Ng, S.M. Sze and Kwok K.** *Physics Of Semiconductor Devices, 3rd Ed.* New Jersey : John Wiley & Sons, Inc., 2007.

10. *p-Type Semiconducting GeSe Combs by a Vaporization-Condensation-Recrystallization Process.* **Seok Min Yoon, Hyun Jae Song, Hee Cheul Choi.** 2010, Advanced Materials, Vol. 22, pp. 2164-2167.

11. *Vaporization-condensation-recrystallization process-mediated synthesis of helical m-aminobenzoic acid nanobelts.* **Yoon SM, Hwang IC, Shin N, Ahn D, Lee SJ, Lee JY, Choi HC.** 23, Suwon : s.n., 2007, Langmuir, Vol. 23, pp. 11875–11882.

12. **Meyers, R.A.** Encyclopedia of Analytical Chemistry. [book auth.] Jürgen Popp and Wolfgang Kiefer. *Raman Scattering, Fundamentals.* Chichester : John Wiley & Sons Ltd, 2000, pp. 13104-13142.

13. **Stokes, D. J.** Principles and Practice of Variable Pressure/Environmental Scanning Electron Microscopy (VP-ESEM). *Principles of SEM.* Chichester : John Wiley & Sons, Ltd, 2008, pp. 17-62.

14. **Förster, H.** UV/VIS Spectroscopy. *Characterization I, Molecular Sieves – Science and Technology.* Berlin, Heidelberg : Springer Berlin Heidelberg, 2004, pp. 337-426.

15. *Synthesis Sol-Gel Derived Highly Transparent ZnO Thin Films for Optoelectronic Applications.* **Wasan R. Saleh, Nada M. Saeed, Wesam A. Twej, Mohammed Alwan.** 2012, Advances in Materials Physics and Chemistry, Vol. 2, pp. 11 - 16.

16. *Raman scattering and infrared reflectivity in GeSe.* **H.R. Chandrasekhar, U. Zwick.** 1976, Solid State Communications, pp. 1509-1513.

17. *Anomalous Raman spectra and thickness-dependent electronic properties of WSe2.* **H. Sahin, S. Tongay, S. Horzum, W. Fan, J. Zhou, J. Li, J. Wu, and F. M. Peeters.** 2013, PHYSICAL REVIEW B, p. 165409.

18. *Raman Spectrum of Graphene and Graphene.* **A. C. Ferrari, J. C. Meyer, V. Scardaci, C. Casiraghi, M. Lazzeri, F. Mauri, S. Piscanec, D. Jiang, K. S.** 18, 2006, PHYSICAL REVIEW LETTERS, Vol. 97, p. 187401.

19. *Lattice strain effects on the optical properties of MoS2 nanosheets.* **Lei Yang, Xudong Cui, Jingyu Zhang, Kan Wang, Meng Shen, Shuangshuang Zeng, Shadi A Dayeh, Liang Feng, Bin Xiang.** 2014, Scientific Reports, Vol. 4, p. 5649.

20. **Panasonic Co.** 3 Failure Mechanism of Semiconductor Devices. s.l. : Panasonic Co, 2009.

21. *New Ultraviolet Photodetector Based on Individual Nb2O5 Nanobelts.* **Xiaosheng Fang, Linfeng Hu, Kaifu Huo, Biao Gao, Lijuan Zhao, Meiyong Liao, Paul K. Chu, Yoshio Bando, Dmitri Golberg.** 2011, Adv. Funct. Mater., Vol. 21, pp. 3907-3915.

22. *Controllable Nondegenerate p-Type Doping of Tungsten Diselenide by Octadecyltrichlorosilane.* **Dong-Ho Kang, Jaewoo Shim, Sung Kyu Jang, Jeaho Jeon, Min Hwan Jeon, Geun Young Yeom, Woo-Shik Jung, Yun Hee Jang, Sungjoo Lee, Jin-Hong Park.** 2, 2015, ACS Nano, Vol. 9, pp. 1099-1107.

23. *Highly Responsive Ultrathin GaS Nanosheet Photodetectors on Rigid and Flexible Substrates.* **PingAn Hu, Lifeng Wang, Mina Yoon, Jia Zhang, Wei Feng, Xiaona Wang, Zhenzhong Wen, Juan Carlos Idrobo, Yoshiyuki Miyamoto, David B. Geohegan, Kai Xiao.** 4, 2013, Nano Lett, Vol. 13, pp. 1649-1654.

24. *Single-Layer MoS2 Phototransistors.* **Zongyou Yin, Hai Li, Hong Li, Lin Jiang, Yumeng Shi, Yinghui Sun, Gang Lu, Qing Zhang, Xiaodong Chen, and Hua Zhang.** 1, 2012, ACS Nano, Vol. 6, pp. 74-80.

25. *Valley physics in tin (II) sulfide.* **A. S. Rodin, Lidia C. Gomes, A. Carvalho, and A. H. Castro Neto.** 2016, Phys. Rev. B, p. 93.

26. *Valley polarization in MoS2 monolayers by optical pumping.* **Hualing Zeng, Junfeng Dai, Wang Yao1, Di Xiao, Xiaodong Cui.** 2012, nature nanotechnology, Vol. 7, pp. 490-493.

27. *Valley-selective circular dichroism of monolayer molybdenum disulphide.* **Ting Cao, Gang Wang, Wenpeng Han, Huiqi Ye, Chuanrui Zhu, Junren Shi, Qian Niu, Pingheng Tan, Enge Wang, Baoli Liu, Ji Feng.** 2012, NATURE COMMUNICATIONS, Vol. 3, p. 887.